Journal of Applied Electrochemistry **31**: 267–273, 2001.

Mass transport characterization of a novel gas sparged photoelectrochemical reactor

J.C. HARPER[1], P.A. CHRISTENSEN[1], T.A. EGERTON[1] and K. SCOTT[2]*
[1]*Department of Chemistry, Bedson Building, University of Newcastle upon Tyne, Newcastle upon Tyne, NE1 7RU, Great Britain*
[2]*Department of Chemical and Process Engineering, Merz Court, University of Newcastle upon Tyne, Newcastle upon Tyne, NE1 7RU, Great Britain*
*(*author for correspondence)*

Received 12 April 2000; accepted in revised form 24 October 2000

Key words: bubble column reactor, mass transport, photoelectrochemical, titanium dioxide, waste water treatment

Abstract

The photoelectrochemical treatment of waste water using immobilised TiO_2 electrodes has been demonstrated to be an attractive alternative to TiO_2 slurry reactors; however, it is generally believed that the diffusion of species to the surface of the catalyst imposes severe mass transfer limitations and hence is a disadvantage of the photoelectrochemical approach. To challenge this view, this paper reports the characterization of the mass transport properties of a novel gas sparged photoelectrochemical reactor. It is shown that passing a constant stream of nitrogen gas through the reactor increased the mass transfer coefficient by an order of magnitude above that in the absence of gas and this was attributed to the turbulent flow regime imposed by rising gas bubbles. It is also demonstrated that the gas–liquid transfer coefficient was greater than that for the rate of liquid diffusion and this has important implications for heterogeneous processes.

List of symbols

c	concentration of solution in optical cell (mol dm^{-3})
C_0	bulk concentration of electrolyte (mol dm^{-3})
D	diffusion coefficient (m^2 s^{-1})
d_e	equivalent diameter (m)
d_R	diameter of reactor (m)
d_s	Sauter mean diameter (m)
F	faradaic constant (C mol^{-1})
g	acceleration due to gravity (m s^{-2})
i_{lim}	limiting current density (A m^{-2})
I_0	incident light intensity (einstein m^{-2} s^{-1})
j_p	photocurrent density (A m^{-2})
k_g	gas mass transfer coefficient (m s^{-1})
k_L	mass transfer coefficient (m s^{-1})
L	minority carrier length (m)
l	optical cell pathlength (cm)
n	number of electrons
q	charge on electron (C)
Q_v	volumetric flow rate (m^3 s^{-1})
r_i	radius of inner cylinder (m)
r_o	radius of outer cylinder (m)
Re	Reynolds number
Sc	Schmidt number
Sh	Sherwood number
u_G	bubble rise velocity (m s^{-1})
W	depletion layer width (m)

Greek symbols

α	absorbtion coefficient of semiconductor (cm^{-1})
ε	molar absorbtion coefficient
ρ_L	density (kg m^{-3})
σ	surface tension (N m^{-1})
ν_L	kinematic viscosity (m^2 s^{-1})

1. Introduction

Wide bandgap semiconductors such as TiO_2 are generally believed to be potentially important catalysts in the removal of organic contaminants from waste water streams [1]. Titanium dioxide has received the most interest as it is cheap, non toxic and its catalytic performance does not diminish with time: in contrast to a number of other semiconductors [2]. The majority of photocatalytic studies utilise small scale slurry reactors which offer a potentially inexpensive solution to the problem of water contamination. However, to minimize electron-hole recombination in the bulk of the semiconductor, the particle must be comparable in size with the

minority carrier length, Lp, which is the average distance an electron vacancy (i.e., postively-charged hole), can migrate in the absence of an electric field before recombination with an electron. This restricts the size of particles that can be utilised effectively to $\leq \sim 0.1$ μm [2], hence the separation of such fine particles from the treated stream is inherently time-consuming and expensive. The problem of post-treatment removal of the catalyst may be overcome by immobilizing the catalyst on a supporting substrate thus avoiding the need to incorporate a filtration unit in a final reactor design [2]. However, electron-hole recombination gives rise to poor conversion efficiencies. The research carried out at Newcastle and elsewhere has shown that by the application of a small potential bias, the rate of the electron hole recombination process can be reduced thus improving the performance of the catalyst [3–7].

A potentially significant limitation associated with immobilised catalysts is that the performance of the reactor may be impaired by poor mass transport and this has limited the application of the technology to date. A standard approach to improving the mass transport of species to a fixed electrode is forced convection and the fact that the most likely counter electrode reaction in a photoelectrochemical reactor will be the reduction of oxygen suggests that the reactor design may benefit from the application of a bubble column reactor approach. In such reactors turbulent flow is induced by rising gas bubbles [8]. As gas passes through the solution, liquid is entrained with the bubbles and produces the distinctive flow pattern as shown in Figure 1. The bubbles and entrained liquid tend to rise up the centre of the column and in particular large bubbles, gravitate towards this region. Smaller bubbles move close to the wall of the reactor and liquid moves in the opposite direction to that in the centre of the reactor. This gives rise to high radial mixing and no liquid phase concentration gradients are found.

The enhancement of mass transfer kinetics in electrochemical reactors by rising gas bubbles has previously been demonstrated by several researchers [9–14]. For example, Fouad et al. [15] investigated the effect of H_2 evolution on the mass transfer rate at nickel electrodes and illustrated that stirring by means of rising gas bubbles was an economical way of achieving the desired hydrodynamic regime. Ibl and coworkers demonstrated that the mass transfer coefficient for the reduction of $Fe(CN)_6^{3-}$ at a Pt disc electrode was enhanced by a factor of ten when the solution was stirred using nitrogen gas [16, 17].

This paper describes the characterization of a novel photoelectrochemical bubble column reactor in the design of which the following criteria were employed:

(a) The reactor should be capable of treating water containing strongly absorbing pollutants since this is characteristic of a number of typical effluent streams arising from industrial activity.

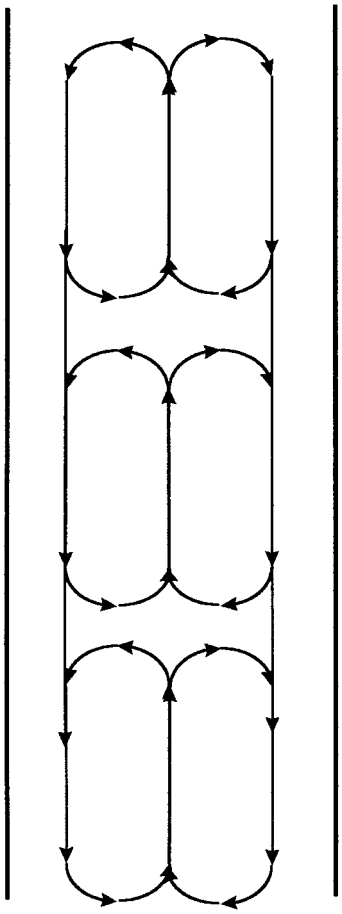

Fig. 1. Cross section of a bubble column reactor illustrating the circulation patterns of liquid.

(b) The mass transport characteristics of the reactor should be as efficient as possible.

(c) The supply of oxidant, (O_2) to the counter electrode should be sufficient to ensure that this process is not rate limiting as has been observed elsewhere [18].

(d) The relative geometry of the lamp and electrode should maximise absorption of light by the latter.

(e) The reactor should be economically feasible and require low maintenance.

The above criteria led to the design of a concentric tube reactor which offered maximum exposure of the photoanode to the u.v. light while minimizing the light path and achieving good mass transport conditions.

2. Experimental details

2.1. *Reactor design*

A cross sectional diagram of the photoelectrochemical reactor is shown in Figure 2(a) and also a schematic representation of the pilot plant reactor is shown in Figure 2(b). The photoelectrochemical reactor was constructed from two concentric Pyrex^{TM} tubes (inner tube: 42 mm external diameter, outer tube: 80 mm internal

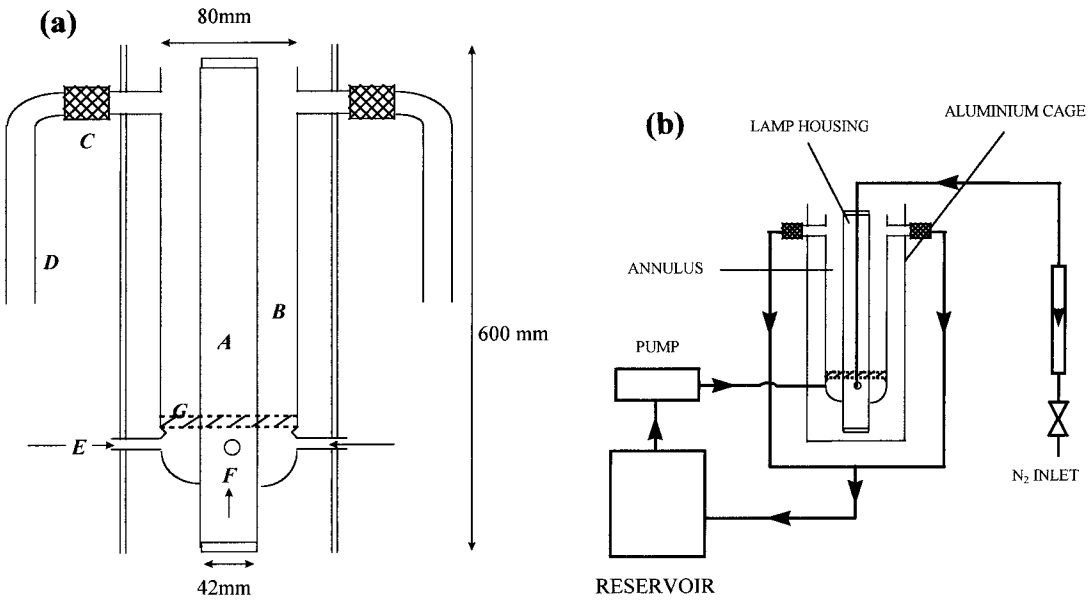

Fig. 2. (a) Cross section of the gas sparged photoelectrochemical reactor. Key: (A) 20 W UVA-UVB lamp, (B) glass reaction vessel, (C) reinforced PTFE hose, (D) outlet port, (E) N_2 inlet, (F) electrolyte inlet and (G) glass gas distributor. (b) Schematic diagram of pilot plant reactor. Reactor operated in a semi-batch mode with electrolyte supplied from a reservior. A co-current stream of nitrogen gas is passed through the reactor vessel via the inlet port (E).

diameter) and had a volume of 0.94 dm^3. Aqueous electrolyte solutions were placed into a feedtank (2 dm^3) and recirculated through the reactor in a multipass mode using a Cole–Palmer 2000 peristaltic pump which produced a maximum volumetric flow rate of 3.22×10^{-5} m^3 s^{-1}.

Figure 3 shows the electrode assembly used in these studies. Nickel gauze, (125 mm × 115 mm, Goodfellows, >99%) was employed as the working electrode and had a surface roughness factor of approximately 2.5 as determined from steady state electrochemical measurements. The auxillary electrode was a platinized steel mesh (130 mm × 115 mm, Goodfellows, >99%) and the platinum black was deposited as described elsewhere [19]. The working and counter electrode cassette consisted of the Ni mesh formed into a cylinder with a platinized steel mesh electrode. The gap between the electrodes was maintained at 2 mm via two concentric nylon spacers. The cassette was inserted into the reactor such that the central wall of the glass vessel and the electrode holder was 0.25 mm.

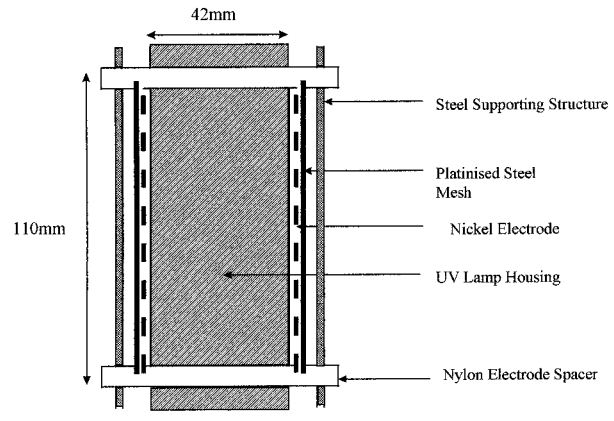

Fig. 3. Electrode assembly and holder.

Gas distribution in bubble column reactors is of particular importance as the choice of distributor can affect gas hold-up, interfacial area and the level of mass transfer [8]. In the present design a 0 grade (20 μm pores) sintered glass disc (Merck Scientific UK) was sealed into the base of the column. These sinters produce small bubbles which increase the gas/liquid interfacial surface area. The bubble size distributions and rise velocities were measured using a Kodak high speed camera with a shutter speed of 500 frames per second.

The photocurrent and hence catalytic activity of the photoelectrode is dependent upon the incident light intensity [20]. According to classical semiconductor theory, the measured photocurrent at a polycrystalline electrode behaves according to the following correlation [21],

$$j_p = qI_0\left[1 - e^{-(\alpha W)/(1+\alpha L)}\right] \quad (1)$$

where j_p is the photocurrent density, I_0 the photon flux, W the depletion layer width, α the absorption coefficient and L is the minority carrier length. Therefore, to maximize catalytic performance, a significant proportion of the output radiation of the lamps must penetrate through solution and interact with the electrode. Aromatic compounds are a major constituent of the effluent in waste water streams resulting from the production of high molecular weight polymers [2]. Therefore, it is crucial to determine the optical densities of aromatic compounds (e.g., nitrophenols), at levels which are representative of those found in industrial effluent. Presented in Table 1 are the optical densities of

Table 1. Absorbtion data of 2,4 dinitrophenol in tap water

Concentration /mmol dm^{-3}	Abs.	$L_{1/2}$ /mm
1.000	1.75	1.72
0.500	0.93	3.24
0.25	0.72	4.2
0.10	0.28	10.75
0.050	0.15	20.6

solutions of 2,4 dinitrophenol in tap water. The distance at which the incident light intensity decreases to half its initial value, $L_{1/2}$, is calculated from,

$$L_{1/2} = \ln 2/2.303\varepsilon cl \tag{2}$$

where ε is the molar extinction coefficient, c is the concentration and l the pathlength of the cell. For example, for a 1 mM solution the $L_{1/2}$ value is less than 2 mm. The highly absorbing solutions have profound implications for the design of an efficient reactor; namely that the performance of the catalyst increases with decreasing electrode/u.v. source distance.

2.2. *Electrochemical measurements*

The mass transport coefficient, k_L, was determined using the reduction of ferricyanide to ferrocyanide [22] according to

$$Fe(CN)_6^{3-} + e^- \longrightarrow Fe(CN)_6^{4-} \tag{3}$$

k_L can be expressed as

$$k_L = \frac{i_{lim}}{nFc_0} \tag{4}$$

where i_{lim} is the limiting current density n is the number of electrons, F is the faradaic constant, k_L is the mass transfer coefficient and c_0 is the initial concentration of the oxidized species.

The electrolyte employed was: 1×10^{-3} mol dm^{-3} potassium ferricyanide (Aldrich, >99.9%), 5×10^{-3} mol dm^{-3} potassium ferrocyanide (Aldrich, >99.9%) and 0.5 mol dm^{-3} potassium carbonate (Fluka, >99%). All potentials are quoted with respect to the Ag/AgCl reference potential. Electrochemical measurements were made using either a Sycopel AEW2 potentiostat (max. current load ≈200 mA) or a potential/current controller constructed within the department (max. current load ≈2 A).

3. Results and discussion

Given the constraints discussed above, it was clearly necessary to minimize the distance between the inner wall of the reactor and the photoanode (to maximize incident u.v.) and also to minimize the distance between the photoanode and the counter electrode (to minimize ohmic loss). It was also necessary to use low flow rates in order to achieve relatively high residence times to maximize pollutant oxidation. Under these conditions, the liquid flow hydrodynamic regime is typically laminar.

It has been shown, Pletcher et al. [23], that expanded mesh electrodes, which cause local variations in fluid direction and velocity, can act as turbulence promoters. The rate of mass transfer was shown to be sensitive to the geometry of the mesh with fine mesh giving the greatest enhancement and in extreme cases the mass transfer coefficient, in comparison with plate electrodes, can increase by one order of magnitude.

The effect of the mesh electrodes used in these studies upon the mass transport properties was first investigated. The limiting current density was measured as a function of volumetric flow rate, Q_v without gas sparging and the associated values of k_L were derived from Equation 4. Figure 4 shows these mass transfer coefficients, k_L, and Reynolds number, Re, as a function of flow rate. The Reynolds number was calculated from the following expression:

$$Re = \frac{ud_R}{v_L} \tag{5}$$

where u is the solution flow velocity, d_R is the diameter of the reactor and v_L the kinematic viscosity of the solution. For an annular reactor the diameter, d_R, can be expressed as an equivalent diameter, d_e, given by [24],

$$d_e = 2(r_o - r_i) \tag{6}$$

where r_i is the radius of the inner and r_o the radius of the outer cylinder. Despite enhancements due to mesh electrodes, it is clear that, under practical operating conditions, increasing the flow velocity will not achieve $Re > 2000$. That is, the rate of mass transport to the electrodes cannot be sufficiently enhanced by the use of mesh electrodes alone.

Therefore, we investigated the additional benefits associated with gas sparging. Figure 5 demonstrates the effects of different N_2 gas flow rates upon k_L. For convenience, the gas flow rate is expressed as the volume fraction in the solution. The values of k_L, approaching 10^{-4} m s^{-1}, an order of magnitude higher than those achieved with our mesh alone, are very high and would only be achieved at high Reynolds numbers. Clearly the use of a co-current stream of N_2 has a marked beneficial effect upon k_L and its value at the highest gas/liquid fraction is approximately twenty times greater than values shown in Figure 4. Indeed, the minimum gas flow used in this study produced an approximate ten fold increase in k_L. Therefore the anticipated high rates of mass transport have been achieved through the process of gas sparging, although mesh electrodes did not by themselves give the necessary turbulence.

The circulatory flow path of solutions in a bubble column reactor was briefly discussed in the introduction. However, the flow paths are further complicated by the

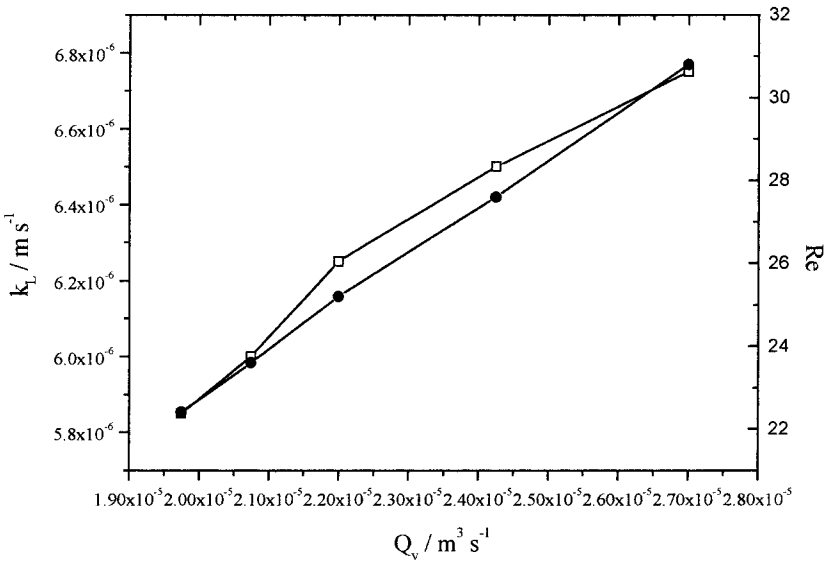

Fig. 4. Calculated mass transfer coefficient (□) and Reynolds (●) number through electrode annulus as a function of volumetric flow rate.

presence of the electrode assembly. Hence, bubble flow paths were examined with the use of high speed camera. Although it is not the purpose of this paper to present a detailed analysis of these flow patterns, the observations show that the stream of bubbles in the centre of the reactor rise vertically with uniform ascent velocities. However, the electrode assembly disturbs the flow path of the gas, and in the region of the electrodes the flow pattern is modified. Localized eddies are produced and the bubbles have a wide distribution of rise velocities. Therefore a simple analysis of the effect on the hydrodynamic properties by parameters such as gas velocities although only strictly applicable in the central region of the reactor permits the correlation of bubble properties with electrode performance. It is also an important procedure in characterizing reactor operation in slurry mode.

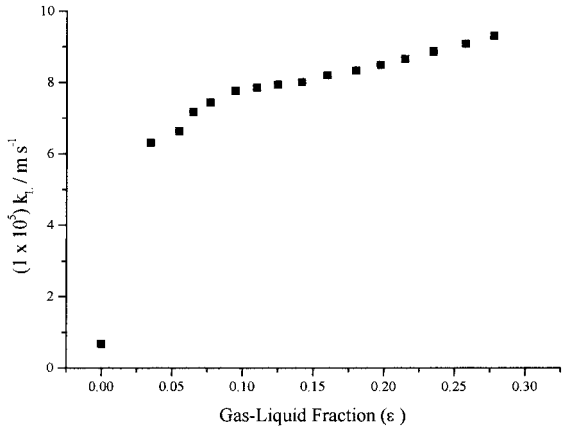

Fig. 5. Mass transfer coefficient as a function of gas–liquid fraction (ε). Volumetric flow rate 2×10^{-5} m^3 s^{-1}.

Mass transfer coefficients are expected to increase with increasing bubble size and rise velocity. Mass transfer depends on Reynolds number which is related [8] to bubble rise velocities, u_G, by

$$Re = \frac{u_G d_R}{v_L} \tag{7}$$

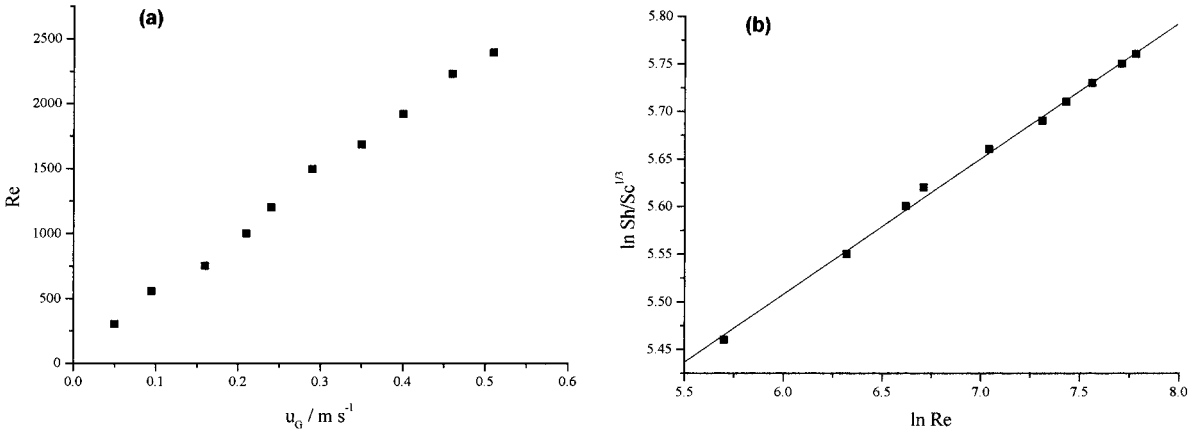

Fig. 6. (a) Dependence of Reynolds number upon bubble rise velocity. Volumetric flow rate 2×10^{-5} m^3 s^{-1}. (b) Mass transfer correlation of reactor. Reynolds numbers calculations based upon the rise velocity of the N_2 gas bubbles.

These results are presented in Figure 6(a). However, for the purposes of the design it is more appropriate to express them in the form of Sherwood numbers

$$Sh = 97.7\,Re^{0.14}[v_L/D]^{1/3} = 97.7\,Re^{0.14}Sc^{1/3} \quad (8)$$

where *Sh* and *Sc* are the Sherwood and Schmidt numbers [21], respectively. This correlation is shown in Figure 6(b).

In the degradation reactions of interest, molecular oxygen is reduced to the superoxide anion radical according to

$$O_2 + e^- \longrightarrow O_2^{-\bullet} \quad (9)$$

The rate at which this reactant reaches the electrode is governed by two diffusion processes; diffusion of gas into the liquid phase and diffusion within the liquid to the electrode. Assuming that the kinetics of charge transfer are significantly faster than bulk diffusion, the slowest of the two mass transfer processes determines the concentration profile of reactant at the interfacial region.

It is, therefore, necessary to know the effect of gas velocity upon the overall rate of mass transport and in addition to considerations of mass transfer within the liquid we must take into account mass transfer across the gas liquid interface [8]. The flow velocity and hence the residence time of bubbles through the reactor has to be sufficient for the solution to be saturated with gaseous reactant. We have applied the correlations obtained by Akita and Yoshida [25] to estimate the gas–liquid mass transfer coefficient. To do this it is necessary to estimate the bubble size distribution or Sauter mean diameter using the following correlation:

$$\frac{d_s}{d_R} = 26\left(\frac{d_R^2 g\rho_L}{\sigma}\right)^{-0.5}\left(\frac{gd_R^3}{v_L^2}\right)^{-0.12}\left(\frac{u_G}{\sqrt{gd_R}}\right)^{-0.12} \quad (10)$$

The values of calculated were in the range of approximately 3–8 mm, consistent with experimental observations. The mass transfer coefficients were then calculated from,

$$k_g = 0.5\frac{D}{d_s}\left(\frac{v_L}{D}\right)^{1/2}\left(\frac{gd_s^3}{v_L^2}\right)^{1/4}\left(\frac{gd_s^2\rho_L}{\sigma}\right)^{3/8} \quad (11)$$

These values are presented in Figure 7. The gas–liquid mass transfer coefficients are approximately three times greater than the solution to the electrode mass transfer coefficient. We conclude that, for the photoelectrochemical oxidation of dilute solutions, the dissolution of oxygen into the liquid phase is unlikely to be the rate limiting process, provided the gas velocities are not so high as to induce slug flow.

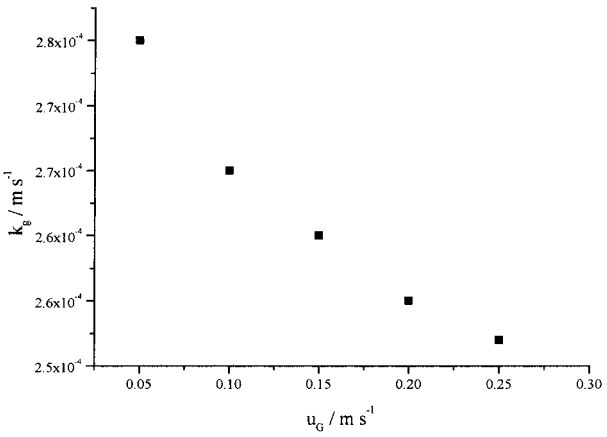

Fig. 7. Dependence of gas–liquid transfer coefficient (k_g) on bubble rise velocity (u_G).

4. Conclusions

The requirements of long residence times and the geometric restrictions imposed by short optical path lengths between the u.v. source and the photoelectrode are likely to lead to poor mass transfer in practical photoelectrochemical reactors. This is particularly so for reactants, such as substituted phenols, with high absorption coefficients. Mass transfer can be improved over and above the enhancement due to mesh electrodes by gas-sparging. Mass transport in a mesh electrode reactor was 20 times greater when sparged. The mass transport coefficients or Sherwood numbers are conveniently correlated with Reynolds number based on bubble characteristics. In oxidation reactors the sparge gas can conveniently be oxygen since, under normal operating conditions, mass transfer at the gas–liquid interface is not rate determining.

References

1. A.M. Mills and S. Le Hunte, *Applied Cat. A* **175** (1998) 221.
2. P.A. Christensen and G.M. Walker, 'Opportunities for the UK in Solar Detoxification', ETSU s/P4/00249/REP (1996).
3. P.A. Christensen, T.A. Egerton, J.C. Harper and J.R. Tinlin, 'Topical Issues in Glasses', Vol. 3, Photons Glasses and Coatings (1991).
4. K.E. Shaw, P.A. Christensen and A. Hamnett, *Electrochim. Acta* **45** (1996) 719.
5. S.A. Walker, P.A. Christensen, K.E. Shaw and G.M. Walker, *J. Electroanal. Chem.* **393** (1995) 137.
6. K. Vinodgopal, S. Hotchandani and P.V. Kamat, *J. Phys. Chem.* **97** (1993) 9040.
7. K. Vinodgopal, U. Stafford, K.A. Gray and P.V. Kamat, *J. Phys. Chem.* **98** (1994) 6797.
8. W.D. Deckwer, 'Bubble Column Reactors' (Wiley, New York, 1992), and references therein.
9. L.J.J. Jansen and J.G. Hoogland, *Electrochim. Acta* **18** (1973) 543.
10. L.J.J. Jansen and E. Barendrecht, *Electrochim. Acta* **24** (1979) 693.
11. G.H. Sedahmed and L.W. Shemilt, *J. Appl. Elec.* **14** (1984) 123.
12. H. Vogt, *J. Appl. Elec.* **19** (1989) 713.
13. J.M. Bisang, *J. Appl. Elec.* **22** (1992) 585.
14. J.M. Bisang, *J. Appl. Elec.* **23** (1993) 966.
15. M.G. Fouad and G.H. Sedahmed, *Electrochim.* Acta **17** (1972) 665.
16. N. Ibl, *Chemie. Ing. Tech.* **39** (1967) 914.

17. N. Ibl, M.E. Adam, J. Venczel and E. Schalch, *Chemie. Ing. Tech.* **43** (1971) 202.
18. J. Kulas, I. Rousar, J. Krysa and J. Jirkovsky, *J. Appl. Electrochem.* **28** (1998) 843.
19. A.I. Vogel, 'Textbook of Inorganic Quantatative Analysis' (Longman, London, 1978).
20. C.J. King and T.A. Egerton, *J. Oil Col. Chem. Assoc.* **62** (1979) 386.
21. H.O. Finklea, 'Semiconductor Electrodes' (Elsevier, Amsterdam, 1988), 55, Chapter 2.
22. F. Goodridge and K. Scott, 'Electrochemical Process Engineering' (Plenum, New York, 1995).
23. L. Lipp and D. Pletcher, *Electrochim. Acta* **42** (1997) 1101.
24. T.K. Ross and A.A. Wragg, *Electrochim. Acta* **10** (1965) 1093.
25. K. Akita and F. Yoshida, *Ind. Eng. Chem. Proc. Des. Dev.* **13** (1974) 84.